Available online at www.sciencedirect.com
ScienceDirect
Coordination Chemistry Reviews 251 (2007) 1649–1662
COORDINATION CHEMISTRY REVIEWS
www.elsevier.com/locate/ccr

Review

Fascinating inorganic/bioinorganic reaction mechanisms☆

Rudi van Eldik

Institute for Inorganic Chemistry, University of Erlangen-Nürnberg, Egerlandstr. 1, 91058 Erlangen, Germany

Received 31 October 2006; accepted 3 February 2007
Available online 11 February 2007

Contents

Abstract

This review presents recent examples of mechanistic studies performed in our group on the activation of NO and peroxides by Fe(III) complexes, from which fascinating reaction mechanisms in the area of inorganic/bioinorganic chemistry evolved. The mechanistic insight gained is based on information obtained from the application of low-temperature rapid-scan techniques, as well as from the application of high pressure thermodynamic and kinetic measurements through which reaction volume profiles could be constructed.

Keywords: Metal catalyzed autoxidation; NO activation; Peroxide activation; Mechanistic studies

1. Introduction

This review is based on the oral presentation delivered at the 37th ICCC. We have in recent years been involved in mechanistic studies that revealed some fascinating reaction mechanisms as indicated by the title of this contribution. The emphasis of the presentation will be on the details of the mechanisms we have studied and why we consider them to be fascinating. The sequence followed in this presentation is the one adopted for the oral presentation. We start off with some general remarks on mechanistic studies in inorganic/bioinorganic chemistry and then discuss the role of solvent exchange reactions and their mechanisms in controlling the reactivity of coordination complexes. As an example of reactivity, we discuss the catalytic activity of aquated metal ions in autoxidation reactions. We then turn to a discussion of the activation of NO in which we focus on Fe(III) porphyrins and cytochrome P450. The mechanistic understanding of such processes forms the basis for the next section on the activation of peroxides, which in general involves a much more complex mechanism. Here we start off with cytochrome P450, then turn to Fe(III) porphyrins and finally present a complete catalytic cycle observed for an oxidation process catalyzed by a model complex of cytochrome P450.

☆ Based on a plenary lecture presented at the 37th International Conference on Coordination Chemistry, 13–18 August 2006, Cape Town, South Africa.

E-mail address: vaneldik@chemie.uni-erlangen.de.

0010-8545/$ – see front matter © 2007 Elsevier B.V. All rights reserved.
doi:10.1016/j.ccr.2007.02.004

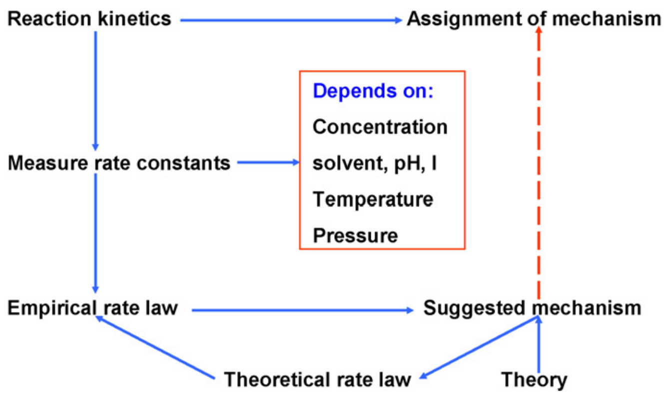

Fig. 1. Schematic presentation of the fundamental principles involved in the elucidation of reaction mechanisms through kinetic and theoretical considerations.

1.1. Selected approach

Our approach is a kinetic-mechanistic one since the reactivity of metal complexes can only be quantified through a kinetic approach. The application of fundamental reaction kinetics has the advantage that not only information on the reactivity of a metal complex can be obtained from the empirical rate law, but in addition mechanistic information can be gained from a systematic variation of chemical and physical variables. In the latter case, temperature and pressure effects can through the application of the transition state theory reveal important mechanistic information in terms of the nature of the transition state based on activation enthalpy, entropy and volume data. A schematic presentation of the fundamental approach in kinetic-mechanistic studies is given in Fig. 1. In order to come as close as possible to the 'real' mechanism, it is essential to gain as much as possible information from the empirical rate law, activation parameters, chemical knowledge on the studied system, evidence for possible intermediates, and a theoretical analysis of the suggested mechanism and proposed transition state. In this respect, based on experience gained over many years, the application of high pressure thermodynamic and kinetic techniques can reveal crucial mechanistic information through the construction of volume profiles for chemical processes. Such profiles not only complement free energy profiles for the studied reactions but further enable a chemical picture to be visualized on the basis of partial molar volume changes that occur along the reaction coordinate. Numerous examples of such profiles are now available, and they have clearly demonstrated the ability of such profiles to contribute to the elucidation of inorganic, organometallic and bioinorganic reaction mechanisms [1]. Two schematic volume profiles for simple bond formation and ligand substitution reactions are shown in Fig. 2. For those interested in inorganic and bioinorganic mechanisms, we refer to a special (June 2005) issue of Chemical Reviews devoted to this topic [2].

1.2. Water exchange reactions

Water exchange reactions, or solvent exchange reactions in a more general sense, are the most fundamental substitution processes that a metal ion in solution can undergo. Although it is a totally symmetric reaction that involves no net chemical change, it is a dynamic process that controls the reactivity of the metal center in terms of ligand substitution and complex-formation reactions, as well as the activation of small molecules by the metal center which first involves the coordination of the small molecule to the metal center prior to the actual activation step. When a metal salt such as $Fe(NO_3)_3$ is dissolved in acidic aqueous solution, it dissociates into aquated Fe(III) and nitrate ions. The aquated Fe(III) ion consists of six water molecules in the first coordination sphere bound to the Fe(III) center, surrounded by at least 12 water molecules in the second coordination (first solvation) sphere that are hydrogen bonded to those in the first coordination sphere (see schematic presentation in Fig. 3). The water molecules exchange at a rate of ca. $10^2\ s^{-1}$ at 25 °C between the first and second coordination spheres in acidic medium, i.e., in the absence of the formation of hydroxo complexes since hexa-aqua-iron(III) is a cationic acid. Such water exchange rate constants can be measured using O^{17}-NMR techniques as a function of temperature and pressure [3], from which mechanistic information on the water exchange process can be obtained. It is in this respect that volume profile analysis has become a very reliable technique to assign the mechanism of solvent exchange reactions, based on the different profiles expected for the different type of exchange mechanisms (see Fig. 4).

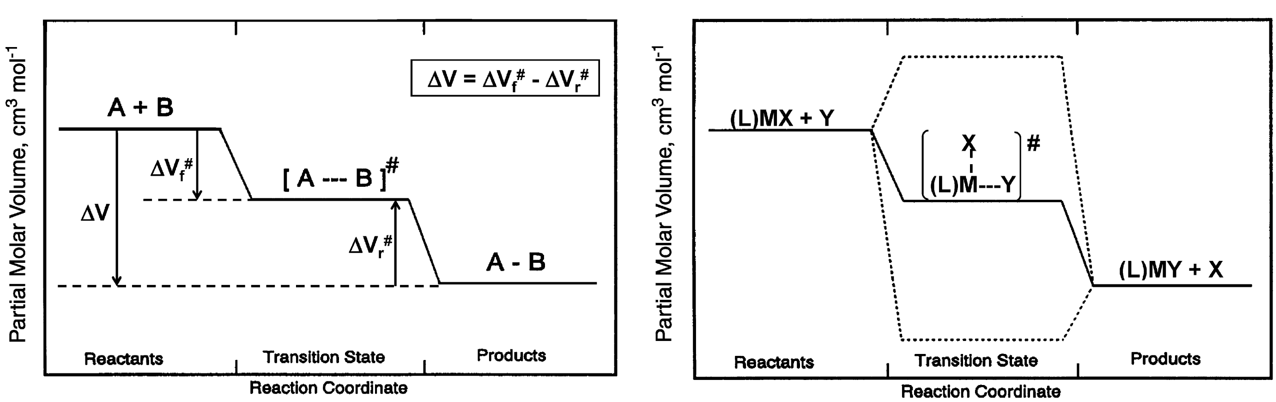

Fig. 2. Schematic volume profiles for simple bond formation (left) and ligand substitution (right) processes. The doted lines in the volume profile on the right represent limiting dissociative (upper) and associative (lower) processes.

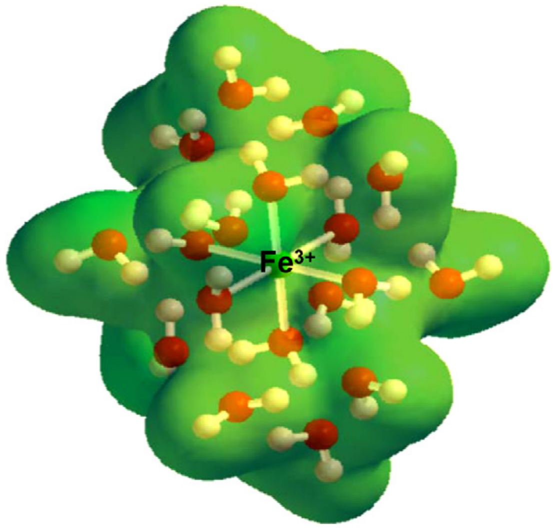

Fig. 3. Schematic presentation of the first and second coordination spheres around the Fe(III) centre in acidic aqueous solution, containing 6 and 12 water molecules, respectively.

Approximately 25 years ago Merbach and Swaddle published their seminal paper on the water exchange mechanism of $[Fe(H_2O)_6]^{3+}$ and $[Fe(H_2O)_5OH]^{2+}$, for which they reported a negative volume of activation for the slow ($10^2\ s^{-1}$ at 25 °C) water exchange on $[Fe(H_2O)_6]^{3+}$ and a positive volume of activation for the much faster ($10^5\ s^{-1}$ at 25 °C) water exchange on $[Fe(H_2O)_5OH]^{2+}$ [4]. These results were interpreted in terms of an I_a and I_d mechanism, respectively, whereby the changeover in mechanism is caused by the *trans* labilization effect of coordinated hydroxide. In addition, the lower electrophilicity of the metal center in the hydroxo complex also disfavors an associative reaction mode. We are aware of the fact that computational chemists have been trying to model this reaction in order to account for the large acceleration and changeover in mechanism observed for the hexa-aqua and monohydroxo complexes. Rather recently we succeeded in modeling these water exchange reactions with DFT calculations, and the calculated

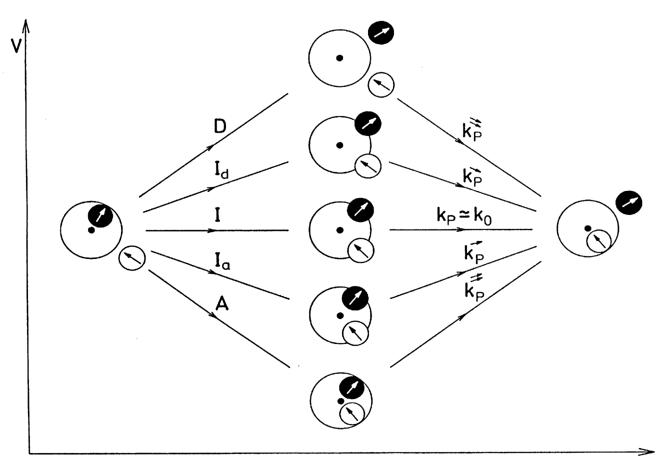

Fig. 4. Schematic volume profiles for solvent exchange on a solvated metal ion following a limiting associative (A), interchange (I) or limiting dissociative (D) mechanism (from bottom to top).

energy profiles and transition state structures are presented in Fig. 5 [5]. Both profiles show evidence for the formation of stable seven- and five-coordinate intermediates, respectively, and the corresponding exchange mechanisms are suggested to be of the limiting associative (A) and limiting dissociative (D) type, respectively. This changeover in mechanism has also been documented for Rh(III), Ir(III), Cr(III) and Ru(III) on the basis of experimental evidence [6].

1.3. Metal ion catalysis

Aquated metal ions can have a strong catalytic effect on autoxidation reactions. Approximately a decade ago there was a strong interest in the formation of acid rain and the effect it had on the environment. One source of acid rain came from SO_2 effluents from coal-fired power plants. Within the European Eurotrac Project [7] various groups investigated the formation mechanism of acid rain, from which it turned out that aqueous phase chemistry in cloud and rain water played a dominant role in the conversion of bisulfite to bisulfate. Under these conditions, trace metal impurities of Fe, Mn, and Co were shown to be extremely efficient catalysts [8]. The cartoon in Fig. 6 illustrates the idea that the spontaneous reaction is very slow (hedgehog), whereas the catalyzed reaction is fast (rabbit). The oxidation reaction hardly occurs over more than 100 min in the absence of metal ions, and is over within a few minutes on the addition of a Fe(III) salt [9]. This demonstrates that the addition of metal ions induces the autoxidation reaction, and detailed mechanistic studies revealed that metal ions in a higher oxidation state can induce the formation of sulfite radicals that in turn can propagate a chain reaction as shown in Scheme 1 [9]. A crucial question concerns the recycling of the catalyst, i.e., the re-oxidation of the reduced metal ion $M^{(n-1)+}$. Detailed studies indicated that species such as $SO_5^{\bullet -}$ and HSO_5^- are strong oxidants and able to re-oxidize the metal ion to complete the catalytic cycle. Thus, in terms of Fe^{3+} as catalyst, the redox cycling of Fe(II/III) can be accounted for by the reaction sequence outlined in Scheme 2. It follows that Fe(III) can induce the formation of the sulfite radical, whereas the combination of bisulfite and oxygen can lead to the re-oxidation of Fe(II) as summarized in Scheme 3 [9]. The overall complex reaction mechanism can be presented in a schematic way as shown in Scheme 4 [7], in which the redox cycling of the metal ion controls the efficiency of the interaction of the various sulfur-oxides in solution. This general scheme was found to hold for almost all the metal ions studied [8].

In order to demonstrate the efficiency of such a redox cycling mechanism in the presence of bisulfite and dioxygen, an experiment was designed to demonstrate the catalytic activity of Co(III), Fe(III) and Ni(III) during the autoxidation of bisulfite [10]. In this experiment the metal ion in the higher oxidation state is reduced by bisulfite (which is oxidized to bisulfate) that is accompanied by a characteristic color change. On shaking the solution, dioxygen from above the solution is dissolved and induces the back oxidation reaction of the reduced metal ion. This reaction does not occur in the absence of bisulfite. In this way the redox cycling of metal ions in rain and cloud water

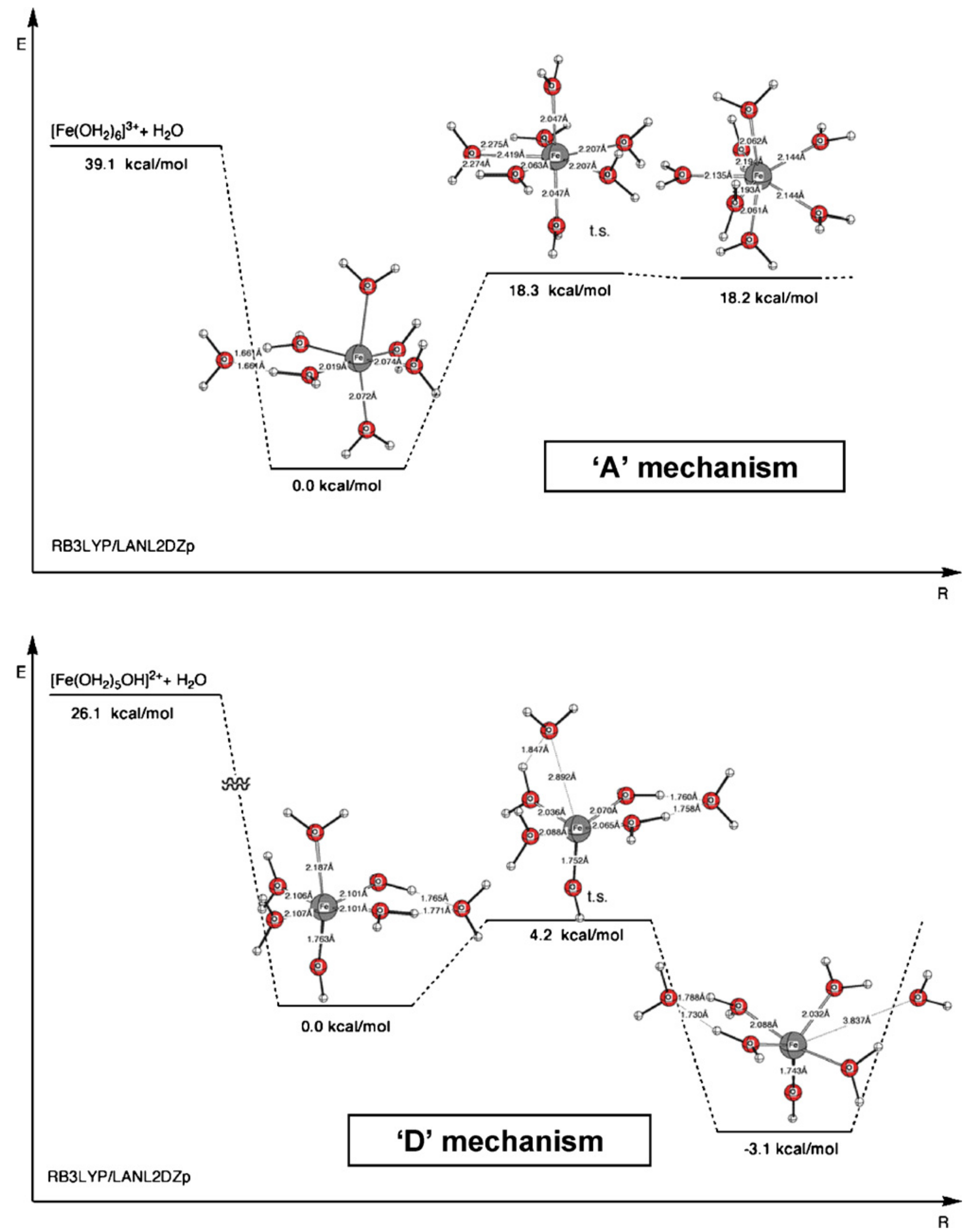

Fig. 5. Energy profiles for water exchange on $[Fe(H_2O)_6]^{3+}$ (top) and $[Fe(H_2O)_5OH]^{2+}$ (bottom) [5].

can be accounted for in terms of the varying concentration of bisulfite (from dissolved SO_2) and dioxygen.

2. NO activation by Fe(III) complexes

In this section we summarize our most recent work on NO activation by Fe(III) porphyrins, cytochrome P450 and functional models.

2.1. Fe porphyrins

The introduction of a porphyrin chelate around a Fe(III) center induces electron density on the metal center and labilizes the coordinated water molecules in the axial position in aqueous medium. This labilization can be nicely studied by O^{17}-NMR as shown schematically for three different porphyrins in Scheme 5 [11]. From the temperature dependence of the NMR line broadening, the water exchange rate constant and the activation enthalpy and entropy values can be determined. The water exchange rate constants are all around $10^6\,s^{-1}$ at 25 °C for the studied complexes, i.e., ca. 10^4 times faster than water exchange on the hexa-aqua system. The activation entropies are all in the range of $+100\,J\,K^{-1}\,mol^{-1}$ and support a dissociative exchange process. By selecting an appropriate temperature, the pressure dependence of the exchange rate constant can be determined as demonstrated in Fig. 7. The calculated volumes of activation are all significantly positive and further underline the operation of a dissociative interchange (I_d) or even a limiting dissociative (D) mechanism in the case of the TMPS complex [11].

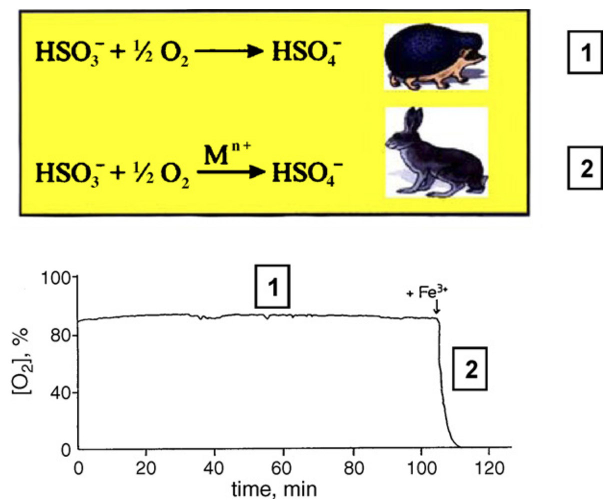

Fig. 6. A cartoon to illustrate the effect of metal ions on the autoxidation of bisulfite (upper part), and the effect of the addition of traces of Fe^{3+} on the consumption of dioxygen (lower part) [8].

OVERALL REACTION:

$HSO_3^- + 1/2\ O_2 \text{ -----------> } SO_4^{2-} + H^+$

INITIATION:

$M^{n+} + HSO_3^- \text{ -----------> } M^{(n-1)+} + SO_3^{\cdot -} + H^+$

PROPAGATION:

$SO_3^{\cdot -} + O_2 \text{ -------------> } SO_5^{\cdot -}$

$SO_5^{\cdot -} + HSO_3^- \text{ -----------> } HSO_5^- + SO_3^{\cdot -}$

OXIDATION:

$HSO_5^- + HSO_3^- \text{ -------------> } 2SO_4^{2-} + 2H^+$

TERMINATION:

$SO_3^{\cdot -} + SO_3^{\cdot -} \text{ -------------> } S_2O_6^{2-}$

$SO_3^{\cdot -} + SO_5^{\cdot -} \text{ -------------> } S_2O_6^{2-} + O_2$

$SO_5^{\cdot -} + SO_5^{\cdot -} \text{ -------------> } S_2O_6^{2-} + 2O_2$

Scheme 1.

$Fe(III) + HSO_3^- \rightarrow Fe(II) + SO_3^{\cdot -} + H^+$ slow

$SO_3^{\cdot -} + O_2 \rightarrow SO_5^{\cdot -}$

$Fe(II) + SO_5^{\cdot -} + H^+ \rightarrow Fe(III) + HSO_5^-$

$Fe(II) + HSO_5^- \rightarrow Fe(III) + SO_4^{\cdot -} + OH^-$

$Fe(II) + SO_4^{\cdot -} \rightarrow Fe(III) + SO_4^{2-}$

$SO_5^{\cdot -} + HSO_3^- \rightarrow HSO_5^- + SO_3^{\cdot -}$

$SO_5^{\cdot -} + HSO_3^- \rightarrow SO_4^{2-} + SO_4^{\cdot -} + H^+$

Scheme 2.

Oxidation of HSO_3^- by Fe(III):

$Fe(III) + HSO_3^- \rightarrow Fe(II) + SO_3^{\cdot -} + H^+$

$Fe(III) + SO_3^{\cdot -} \rightarrow Fe(II) + SO_3$

$SO_3 + H_2O \rightarrow HSO_4^- + H^+$

Oxidation of Fe(II) by HSO_3^-/O_2:

$Fe(II) + SO_5^{\cdot -} \rightarrow Fe(III) + SO_5^{2-}$

$Fe(II) + SO_5^{2-} + H^+ \rightarrow Fe(III) + SO_4^{\cdot -} + OH^-$

$Fe(II) + SO_4^{\cdot -} \rightarrow Fe(III) + SO_4^{2-}$

Scheme 3.

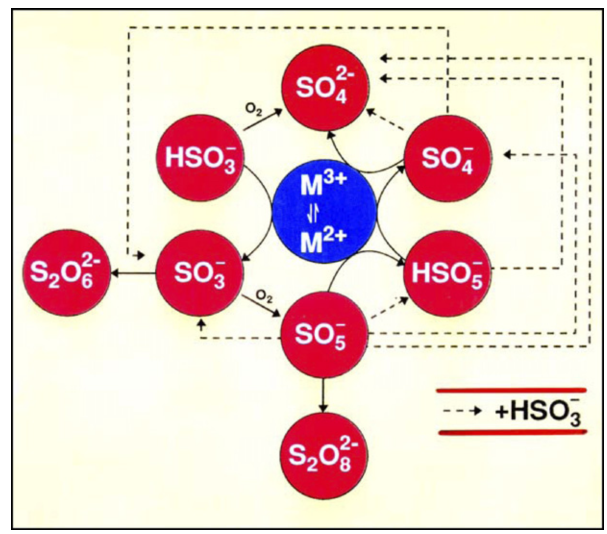

Scheme 4.

Further investigations on the $[Fe^{III}(TMPS^{4-})(H_2O)_2]$ complex indicated that it exhibits a pK_a value of 6.9 and undergoes a change in spin-state from a spin admixed ($S = 5/2$, 3/2) state at pH 5 to a high-spin ($S = 5/2$) state at pH 9. In addition, no water exchange reaction could be detected at pH 9, from which it was concluded that under such conditions a five-coordinate hydroxo complex is formed (see Scheme 6) [12]. The reversible binding of NO to this complex as a function of pH can therefore

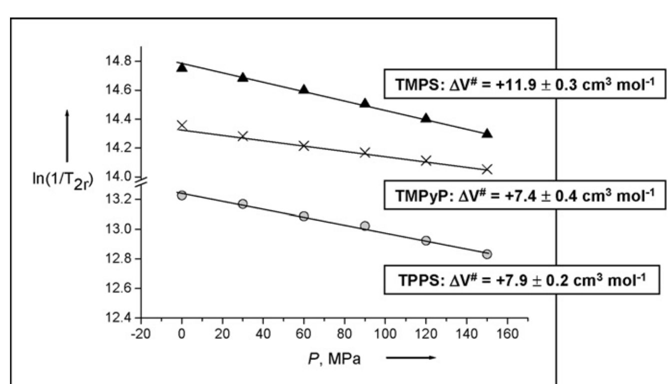

Fig. 7. Effect of pressure on the water exchange reaction for the different Fe(III) pophyrins shown in Scheme 5 [11].

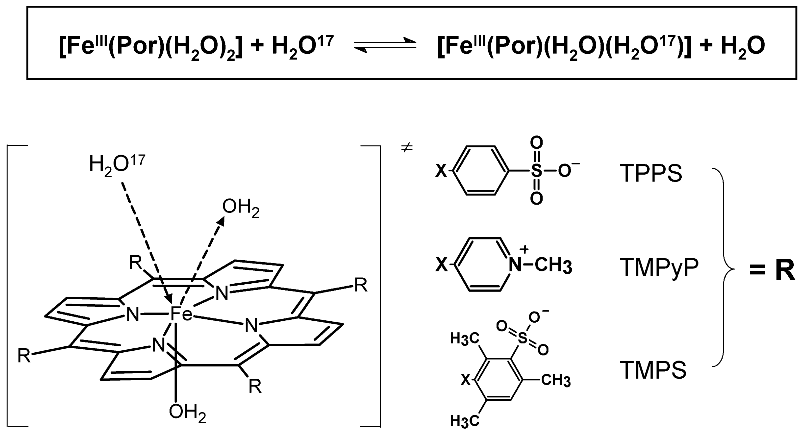

Scheme 5.

we formulated as in Scheme 7. The kinetic data and activation parameters for both the 'on' and 'off' reactions as a function of pH clearly indicate a changeover in mechanism, from dissociative at pH 5 to associative at pH 9. This is nicely demonstrated by the corresponding volume profiles reported in Fig. 8. The reaction product is in both cases a diamagnetic Fe^{II}–NO^+ complex, demonstrating that the coordination of NO indeed involves activation of NO through the formal oxidation of NO by the metal center. Furthermore, this implies that the reaction at high pH involves a high-spin to low-spin changeover which contributes to the overall volume collapse observed for this process [12]. A comparison of the activation volume for water exchange with that found for the binding of NO to the diaqua complex at pH 5 shows that these values are indeed very similar and suggest that the water exchange process controls the rate and mechanism of the binding of NO. The activation barrier for the coordination of NO to the vacant coordination site of the five-coordinate high-spin hydroxo complex was suggested to be the spin change barrier that must be overcome during the binding process.

Similar results were reported for related porphyrin complexes for which the overall charge on the porphyrin was varied from −8 to +8 by introducing different substituents on the porphyrin ring, with the result that the pK_a values of the diaqua complexes varied from 9.2 to 5.0, respectively [13,14]. By way of comparison, the volume profiles for the reversible binding of NO to the −8 charged porphyrin complex as a function of pH, is reported in Fig. 9 [13]. A schematic presentation of the mechanism for the coordination of NO to this complex as a function of pH is presented in Scheme 8. Once again a clear changeover in the nitrosylation mechanism as a function of pH is observed.

2.2. Cytochrome P450 and model complexes

The results in the previous section indicate how a change in pH can have a drastic effect on the binding of NO in terms of changing from a six-coordinate, spin-admixed diaqua complex to a five-coordinate, high-spin hydroxo complex by just increasing the pH. A similar situation is encountered in cytochrome

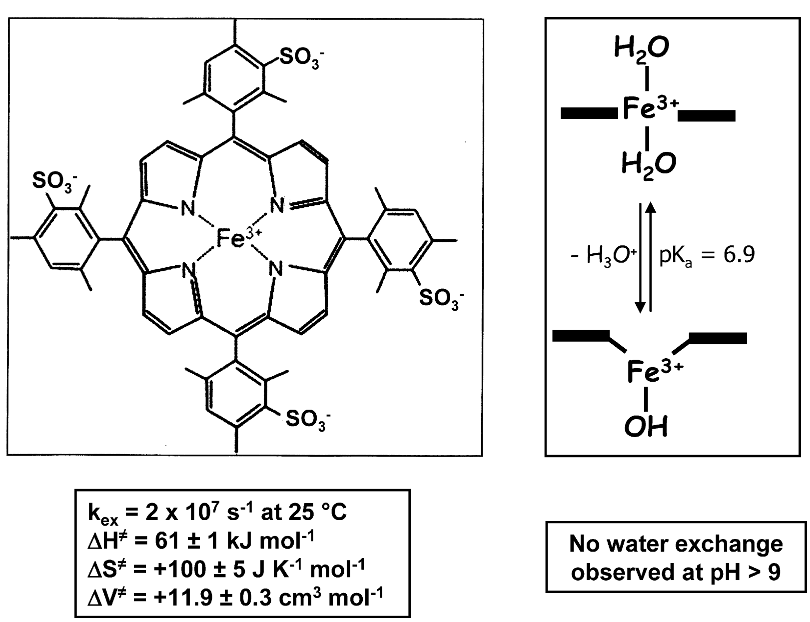

Scheme 6.

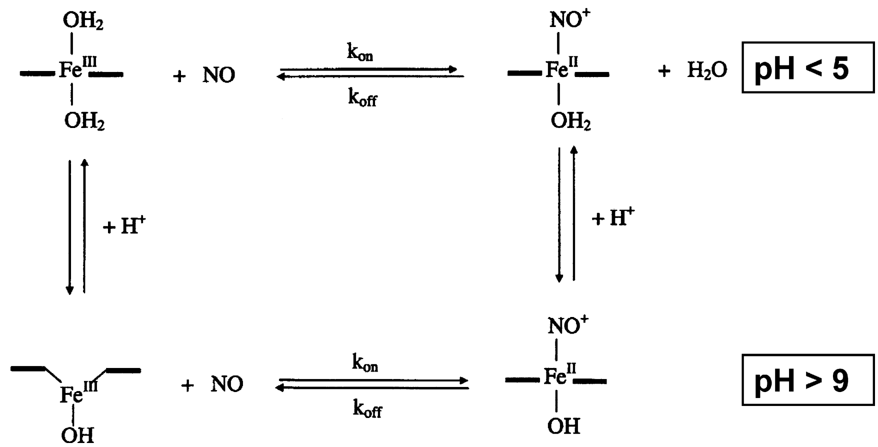

Scheme 7.

P450 not as function of pH, but as function of the absence or presence of a substrate. The resting state of P450 is a six-coordinate, low-spin aqua complex, whereas in the presence of a substrate such as camphor the resting state is converted to a five-coordinate, high-spin complex in which the substrate has entered the active pocket. This is illustrated schematically in Scheme 9. It is well-known that NO inhibits the catalytic activity of P450 by coordinating to the Fe(III) center to form a diamagnetic (low-spin), six-coordinate Fe^{II}–NO^{+} complex in the absence and presence of substrate [15 and references cited therein]. Thus, coordination of NO to P450 will involve the binding to a low-spin, six-coordinate complex in the absence of a substrate and to a high-spin, five-coordinate complex in the presence of a substrate, which is comparable to the situation encountered for the Fe(III) porphyrin complexes at low and high pH, respectively.

The rate and activation parameters for the reversible binding of NO to P450 in the absence and presence of camphor as substrate clearly demonstrate that the reactions proceed according to totally different mechanisms. Where the activation entropy and activation volume for the reversible binding of NO to the resting state of P450 in the absence of substrate clearly support the operation of a dissociative mechanism, these parameters for the reversible binding of NO to P450 in the presence of the substrate support the operation of an addition and elimination process, respectively. The volume profiles reported in Fig. 10 nicely demonstrate this point [15]. The large volume increase observed for the binding and release of NO in the case of substrate-free P450 is partly due to the dissociative character of the process and partly due to a change in spin-state from low-spin to high-spin, which is typically accompanied by a volume increase between 12 and 15 $cm^3\ mol^{-1}$ [16]. In the presence of substrate, the binding of NO is accompanied by a decrease in volume typical for a bond-formation process, followed by a further volume decrease associated with a high-spin to low-spin changeover.

Very recently this work was extended to functional models for P450 developed by the group of Higuchi in Nagoya [17] and the group of Woggon in Basel [18]. Fig. 11 presents a comparison of the active site coordination sphere of these model complexes

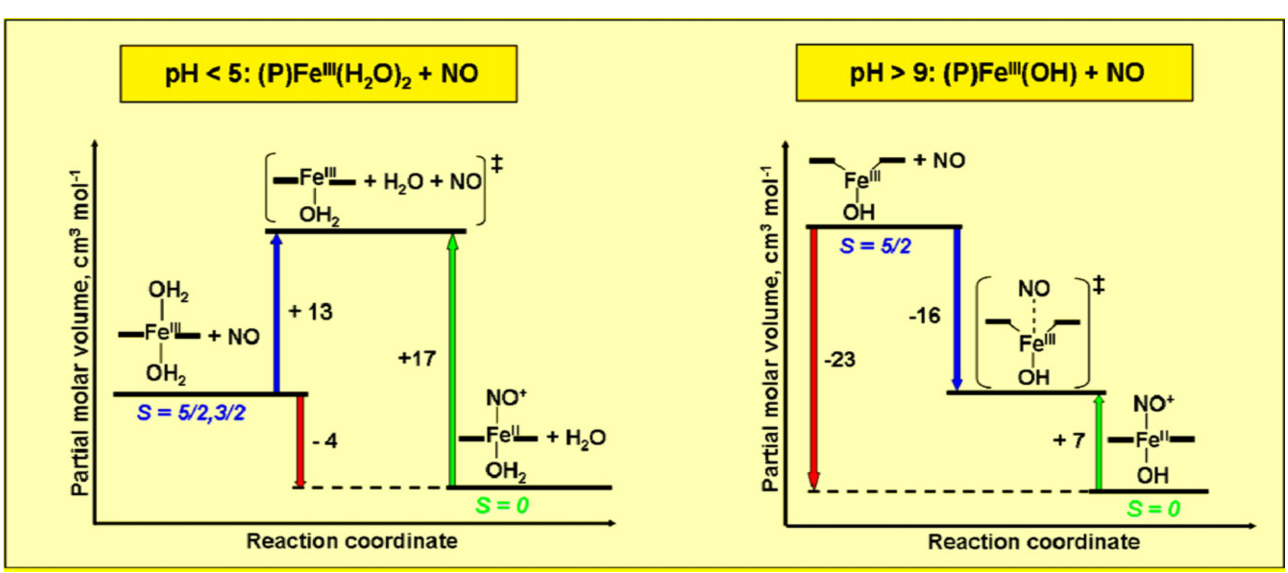

Fig. 8. Volume profiles for the reversible binding of NO to $[Fe^{III}(TMPS^{4-})(H_2O)_2]$ and $[Fe^{III}(TMPS^{4-})OH]$ [12].

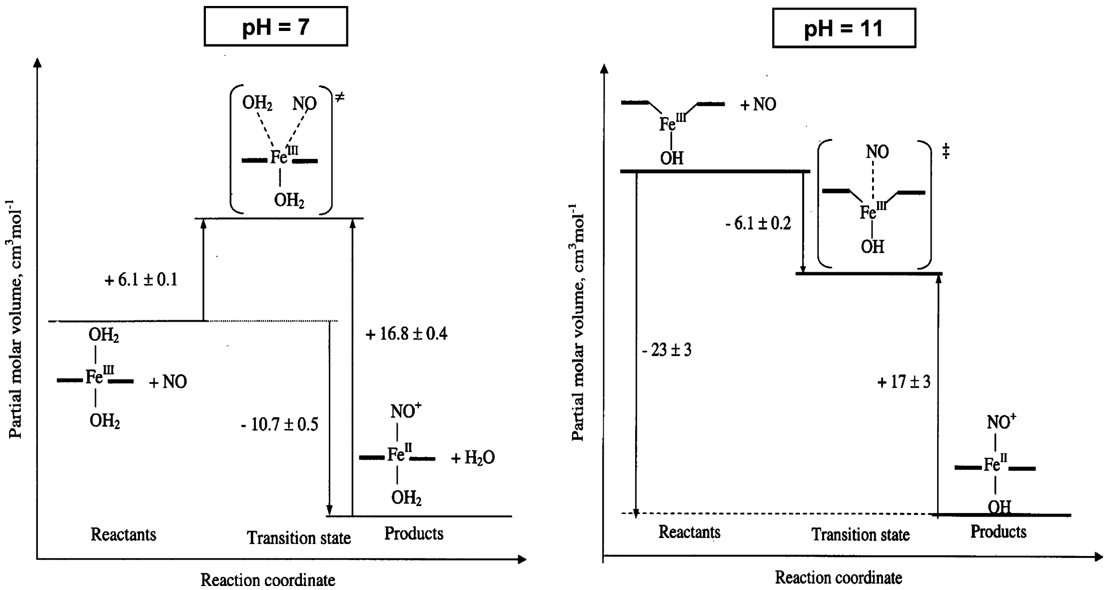

Fig. 9. Volume profiles for the reversible binding of NO to $[Fe^{III}(P^{8-})(H_2O)_2]$ and $[Fe^{III}(P^{8-})OH]$ at pH 7 and 11, respectively [13].

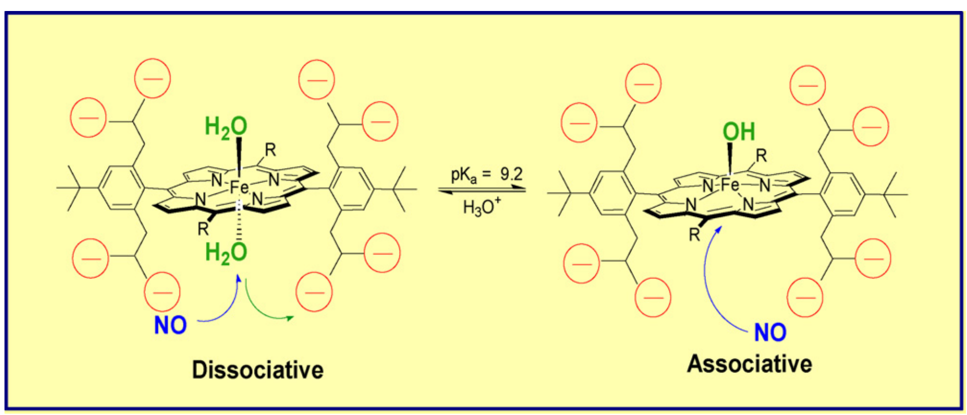

Scheme 8.

and that of cytochrome P450. Higuchi and co-workers prepared a stable low-spin Fe^{III}-porphyrin alkanethiolate complex (SR complex, see complex **1** in Fig. 11), in which the thiolate ligand is sterically protected by bulky pivaloyl groups. It was shown that the SR complex displays similar reactivity to that of cytochrome P450 enzymes and its bulky-protected axial thiolate ligand remains stable during the catalytic cycle. We investigated the mechanistic aspects of reversible binding of NO to the SR complex in coordinating (methanol) and non-coordinating (toluene) solvents [19]. Systematic kinetic studies revealed that the interaction of the SR complex with NO cannot be described as a simple reversible binding of NO to the iron(III) center as it was reported earlier for the $P450_{cam}$/NO system. Even for a low excess of NO, a rather complex reactivity pattern with several reaction steps was clearly observed. Under the conditions of low NO concentrations, NO reversibly coordinates to the SR complex in methanol with a binding rate constant similar to that found for the corresponding reaction with $P450_{cam}$. The NO dissociation rate constant is also of the same order of magnitude as that reported for the $P450_{cam}$/NO system. The activation parameters determined for the formation of the SR–NO complex in methanol suggest a limiting dissociative mechanism that is dominated by the dissociation of a coordinated methanol molecule. Almost a three orders of magnitude higher value for

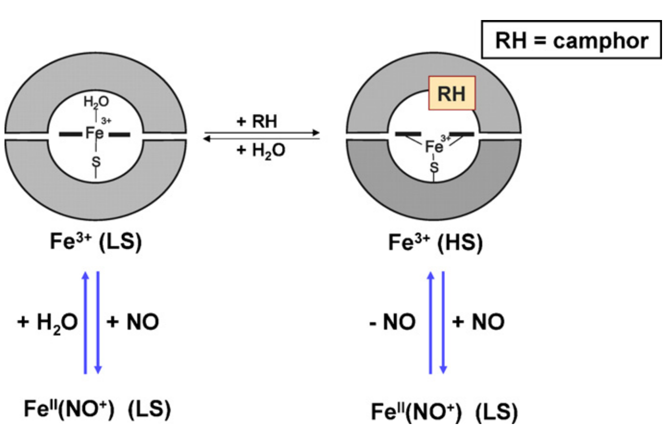

Scheme 9.

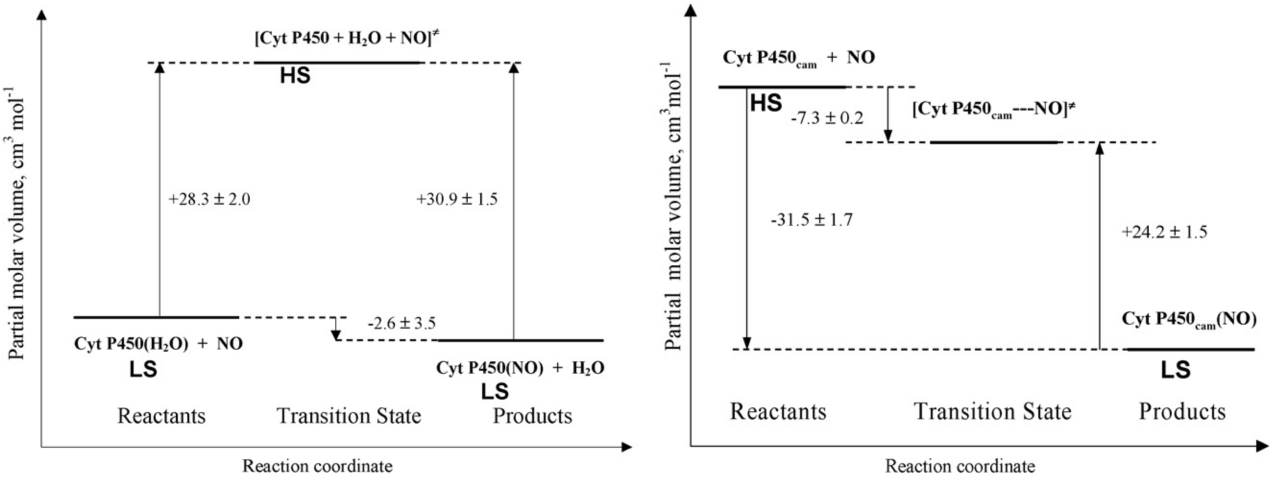

Fig. 10. Volume profiles for the reversible binding of NO to P450 in the absence (left) and presence (right) of substrate [15].

the NO binding rate constant determined for this reaction in a non-coordinating solvent like toluene, clearly supports that the NO binding dynamics is in this case governed by the coordination mode of the iron(III) center.

Under the conditions of an excess of NO, rapid SR–NO complex formation is followed by subsequent slower processes. The second observed reaction can be accounted for in terms of direct attack of a second NO molecule on the sulfur atom of the thiolate ligand in the initially formed SR–NO complex. This leads to the formation of the five-coordinate SR(Fe^{II}) nitrosyl complex, which was characterized by EPR and IR spectroscopy. Although the thiolate ligand in the SR complex is sterically protected by bulky groups, formation of the *S*-nitrosylated derivative under conditions of a large excess of NO does not seem unusual. The following two slower reactions appeared to be strongly accelerated by a large excess of NO or by the presence of higher nitrogen oxides (NO_x) in the reaction medium. They can be accounted for in terms of the dynamic equilibria between higher nitrogen oxides and reactive SR species, which results in the formation of a nitrosyl-nitrite complex of SR(Fe^{II}) as the final product [19].

The complexes developed by Woggon [18] (see **3** and **4** in Fig. 11) have a sulfonate group attached to the axial position of the Fe(III) center and exhibit very similar redox potentials

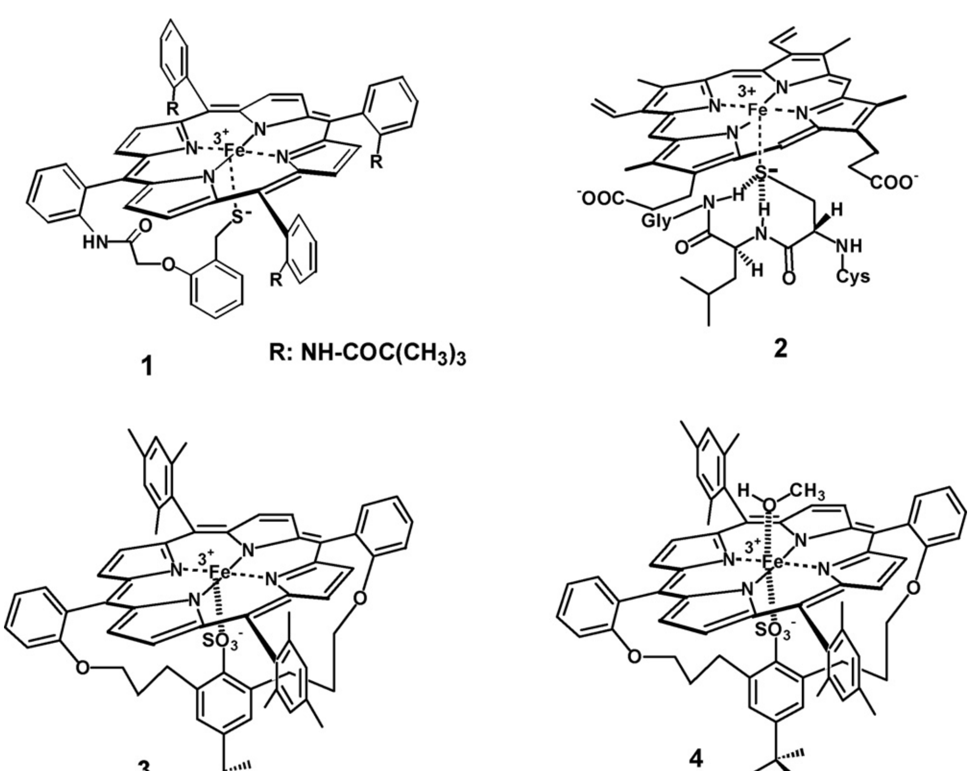

Fig. 11. The active site coordination sphere of $P450_{cam}$ (**2**) model systems (**1** (SR complex), **3** and **4**).

and catalytic activities as found for cytochrome P450. DFT calculations revealed that introduction of the RSO_3^- ligand significantly reduces the negative charge localized on the oxygen that coordinates to the iron(III) center. Therefore, such a system can better mimic the coordination sphere of several native P450 enzymes, in which electron donation from the sulfur atom is also reduced due to the presence of hydrogen bonding between the thiolate ligand and residues of the amino acids in the protein pocket. To investigate the influence of the identity of the proximal and distal ligands on the dynamics of NO binding to this new synthetic model, we performed thermodynamic and kinetic studies on NO coordination to complexes **3** and **4**, in non-coordinating toluene and in coordinating methanol, respectively [20]. In toluene, the five-coordinate, high-spin complex **3**, reminiscent of the camphor-bound $P450_{cam}$ is formed, whereas in methanol the six-coordinate complex **4** should be produced, resembling the resting state of $P450_{cam}$. The model complex **3** displays a NO binding rate constant in a non-coordinating solvent similar to that measured for the NO association reaction of camphor-bound $P450_{cam}$. However, the rate constants for the NO release from the nitrosyl complexes of **3** and camphor-bound $P450_{cam}$ differ by almost **4** orders of magnitude, which results in a significantly lower value of the NO binding constant for **3** at room temperature. However, the binding constant increases significantly on going to lower temperatures and higher pressures, from which the following thermodynamic data was estimated: $K_{NO} = 40\,M^{-1}$ at 25 °C, $\Delta H^\circ = -72\,kJ\,mol^{-1}$, $\Delta S^\circ = -210\,J\,K^{-1}\,mol^{-1}$ and $\Delta V^\circ = -39\,cm^3\,mol^{-1}$. The significantly negative reaction entropy and volume values suggest that NO binding to the high-spin iron(III) center is accompanied by a changeover to low-spin (diamagnetic) Fe^{II}–NO^+ product, which is confirmed by spectroscopic observations [20].

Activation parameters found for NO binding to complex **3** and native camphor-bound $P450_{cam}$ support the same mechanism for both reactions, which is dominated by Fe^{III}–NO bond formation accompanied by a change in the iron(III) spin state (from $S = 5/2$ to $S = 0$). However, despite this similarity in the reaction volume and entropy, the volume profiles for NO binding to these complexes (Fig. 12) differ substantially in terms of the position of the transition state, which can reflect different contributions arising from bond formation and change in spin state. In contrast to the volume profile constructed for the reaction between NO and camphor-bound $P450_{cam}$, reversible binding of NO to **3** is described by a "late" transition state for the association reaction and an "early" transition state for the dissociation reaction. This feature is in agreement with relatively slow "on" and fast "off" reactions and results in the much lower binding constant for NO coordination to **3** than to the native $P450_{cam}$ [20].

The NO binding constants determined for the enzyme models **3** and **4** are about **4** orders of magnitude smaller than those found for the native $P450_{cam}$/NO system, which can be explained in terms of the very effective NO dissociation from the nitrosyl complexes of **3** and **4**. Due to the exothermic nature of NO coordination to **3** and **4**, the NO binding constants for these complexes increase significantly with decreasing temperature. This is a general observation noted also for other model enzymes (for instance, the binding of dioxygen to model complexes for hemocyanine and tyrosinase) where intermediate oxidant or substrate-bound species can be stabilized only at very low temperatures. This feature clearly highlights the important role of the enzyme pocket of $P450_{cam}$ in stabilizing the NO^+ state and formation of more stabile nitrosyl complexes at ambient temperature as compared to those observed for many protein free model complexes. Thus, although the ligand substitution behavior of synthetic iron(III) porphyrin complexes can to some extent be regulated by tuning the electronic nature of the porphyrin ring, the identity and number of axial ligands, and selection of experimental conditions (coordinating/non-coordinating solvent, pH, temperature, etc.), comparison of the kinetic and thermodynamic data for the native iron(III)-thiolate hemoproteins with those obtained for protein-free enzyme models clearly high-light the unique features of the protein architecture in controlling the dynamics of NO binding to P450 cytochromes according to their physiological activity.

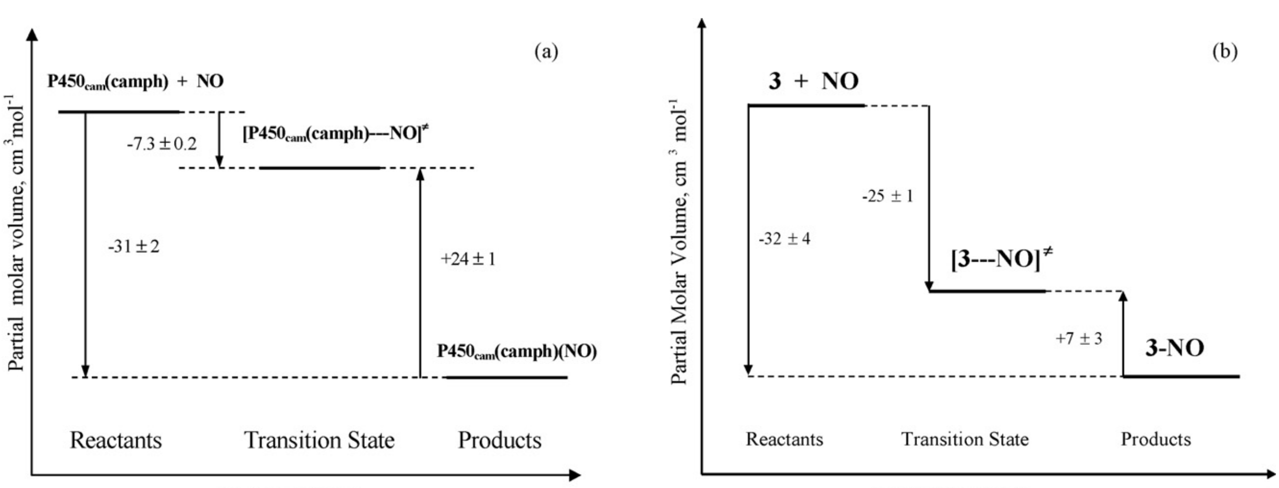

Fig. 12. Comparison of volume profiles for NO binding to (a) camphor-bound $P450_{cam}$ [ref], and (b) complex **3** in toluene [20].

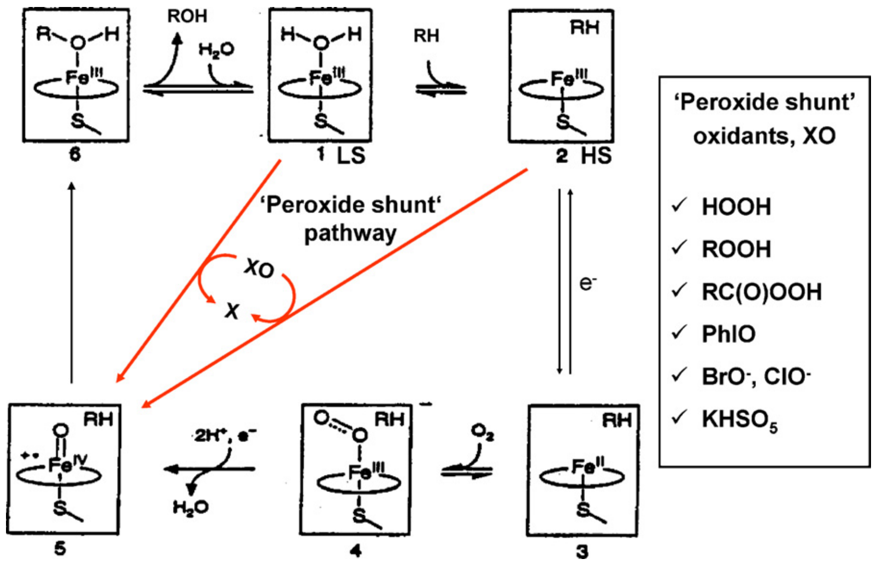

Scheme 10.

3. Peroxide activation by Fe(III) complexes

The Fe(III) porphyrin complexes, cytochrome P450, and the model complexes for P450 discussed in the previous section, all include an iron center of which the coordination number and spin state can be tuned either through the pH, the presence of a substrate or the selected solvent, respectively. The mechanistic understanding of the interaction of NO with these Fe(III) systems under the conditions selected to tune the coordination number and the spin state of the metal center, provides an excellent basis for studying a more complex, multi-step reaction system, viz., the activation of peroxides by such Fe(III) systems. Where in the case of the activation of NO we are only dealing with NO coordination and a subsequent charge transfer process, the activation of peroxide involves coordination of peroxide, subsequent homolysis or heterolysis of the peroxo O–O bond, and formation of high oxidation state iron complexes that are able to oxidize substrate molecules, a reaction step of fundamental interest to many catalytic oxidation processes [21].

3.1. Cytochrome P450

The activation of peroxide by cytochrome P450 is based on the 'peroxide shunt' pathway that short-cuts the oxidation cycle for the overall reaction,

$$RH + O_2 + 2H^+ + 2e^- \rightarrow ROH + H_2O$$

by combining O_2, $2H^+$ and $2e^-$ in the form of H_2O_2 (or as organic peroxides and peroxo acids) as shown schematically in Scheme 10 [22]. Important to note is that the resting state of P450 in the absence and presence of substrate has the properties discussed above for the interaction with NO as outlined

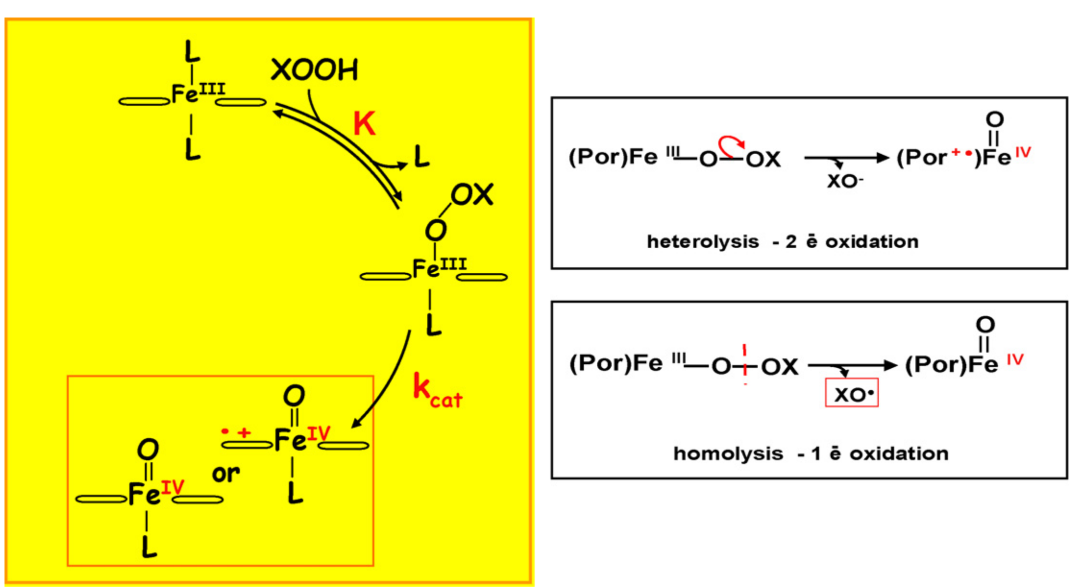

Scheme 11.

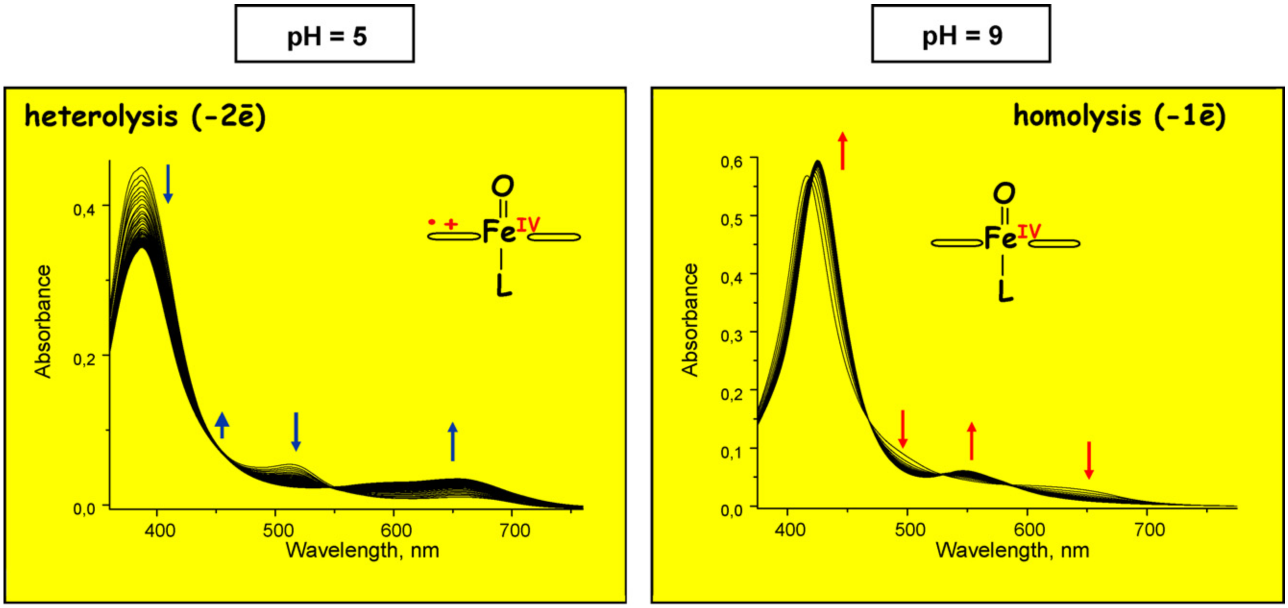

Fig. 13. Spectroscopic evidence for the occurrence of heterolytic and hemolytic bond cleavage during the reaction of [$Fe^{III}(TMPS^{4-})$] with PhIO as a function of pH.

in Scheme 9. Complex **5** in Scheme 10 is the actual species of great interest since this species accounts for the subsequent oxygen-transfer process, a reaction that has received much attention from many researchers [22]. The interaction of peroxo species with the reactant species **1** and **2** will first of all involve rapid binding of peroxide to the Fe(III) porphyrin center (as observed for the reaction with NO), followed by homolytic or heterolytic cleavage of the O–O peroxo bond. This process can be summarized as in Scheme 11. We were surprised to find that the selection between an overall two-electron oxidation process (heterolysis) or an one-electron oxidation process (homolysis) can be tuned by pH as the following example will demonstrate.

3.2. Fe porphyrins

The $Fe^{III}(TMPS^{4-})(H_2O)_2$ complex shown in Scheme 6 has a pK_a value of 6.9. On treating this complex with iodosylbenzene (PhIO), a two-electron oxidation process to form $(Por^{\bullet +})Fe^{IV}{=}O$ occurs at pH = 5, whereas an one-electron oxidation process to form $(Por)Fe^{IV}{=}O$ occurs at pH 9 according to the characteristic UV–vis spectral changes observed for these reactions (Fig. 13). Thus, we again observe a totally different overall redox process by just changing the pH of the solution, i.e., a mechanistic changeover similar to that found for the activation of NO [21]. Similar results were obtained for other oxygen donors such as H_2O_2, *m*-chloroperoxybenzoic acid (*m*-CPBA) and cumene hydroperoxide. Typical spectral changes supporting a one-electron oxidation process (homolysis) are shown in Fig. 14 for the reaction of $Fe(TMPS^{4-})$ with *m*-CPBA. A systematic variation of the *m*-CPBA concentration revealed that the observed first-order rate constant exhibits a saturation behavior on increasing the *m*-CPBA concentration. This is typical for a process that consists of a rapid pre-equilibrium (peroxide binding to the Fe(III) center in Scheme 11) followed by rate-determining cleavage of the O–O bond. In addition, a trap such as ABTS can be used to trap the higher oxidation state oxo complexes as shown in Scheme 12 by following the characteristic absorbance increase at 660 nm for the formation of the $ABTS^{\bullet +}$ radical cation. In this way the overall second-order rate constant for the catalyzed oxidation of ABTS by *m*-CPBA in the presence of $Fe(TMPS^{4-})$ could be determined as a function of temperature and pressure, such that mechanistic information on the oxygen transfer process can be extracted [23]. It is clear from the presented information that only certain steps of the overall catalytic cycle in Scheme 12 can be observed directly under the selected conditions. To reach our goal to observe all reaction steps, we turned to investigations at low temperature in non-

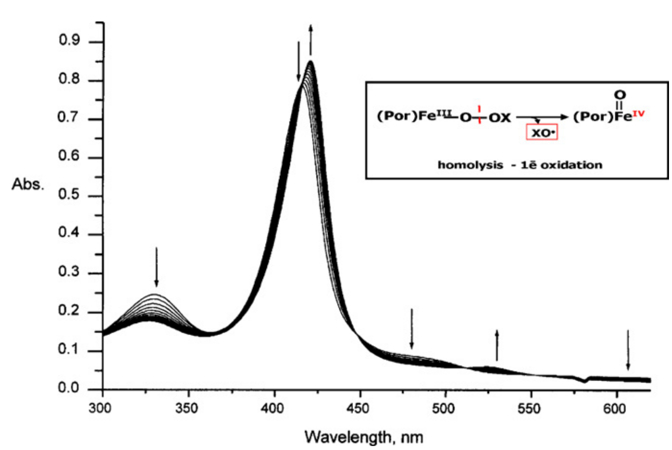

Fig. 14. Spectral changes observed during the reaction of [$Fe^{III}(TMPS^{4-})$] with *m*-CPBA at pH 10. Experimental conditions: [$Fe^{III}(TMPS^{4-})$] = 1×10^{-5} M, [*m*-CPBA] = 5×10^{-5} M, temp. 25 °C.

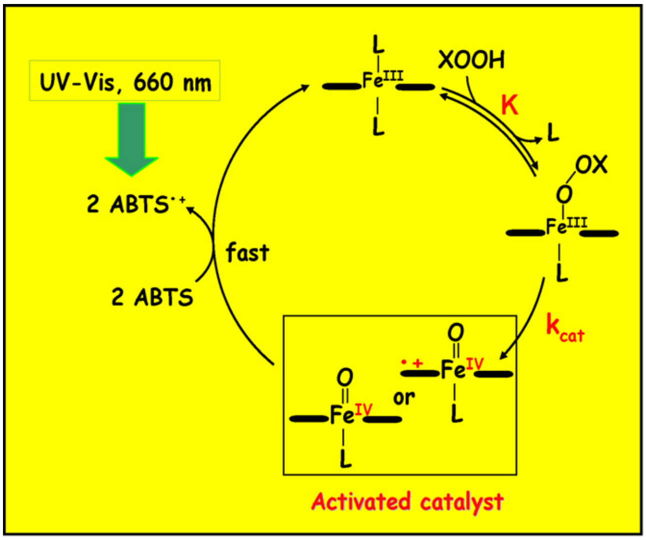

Scheme 12.

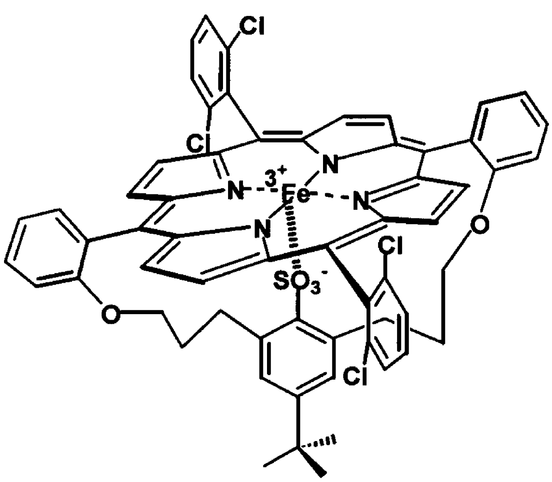

Scheme 13.

aqueous medium in which rapid-scan techniques could be used in order to observe each reaction step separately as illustrated in the following section.

3.3. Catalytic oxidation cycle

For this purpose we used the high-spin, five-coordinate complex prepared by the Woggon group [18] shown in Scheme 13 that exhibits excellent catalytic behavior in epoxidation reactions. We studied the mechanistic behavior of this complex with *m*-CPBA as oxidant in MeCN at −35 °C using a low-temperature stopped-flow system with a rapid-scan detector. We could observe the reversible coordination of *m*-CPBA to the high-spin Fe(III) center, followed by the acid-catalyzed heterolytic cleavage of the O–O bond to form the Fe(IV) porphyrin radical cation that subsequently oxidizes the substrate (1,4-diphenylbutadiene or cis-stilbene in an epoxidation reaction) and fully returns to the Fe(III) starting complex (**1**) (see catalytic cycle shown in Scheme 14. Our biggest surprise was the fact that under the selected conditions the catalyst almost completely returned to its starting state based on the observed spectral changes [24]. Thus all the reaction steps, schematically shown in Scheme 14, could be observed by UV–vis spectroscopy under the selected low temperature conditions.

4. Conclusions

It was our aim with this review to focus on examples of some fascinating inorganic/bioinorganic reaction mechanisms studied in our laboratories over the past few years. Fundamental work on the understanding of the activation of NO by Fe(III) complexes has formed the basis for mechanistic studies on the more complex activation of peroxides, which can now be studied in detail. The work has been very tedious, but we are happy about the progress we could make in this area. Volume profiles have been extremely helpful to clarify some of the essential mechanistic aspects and to elucidate the contribution of spin state changes during such activation processes.

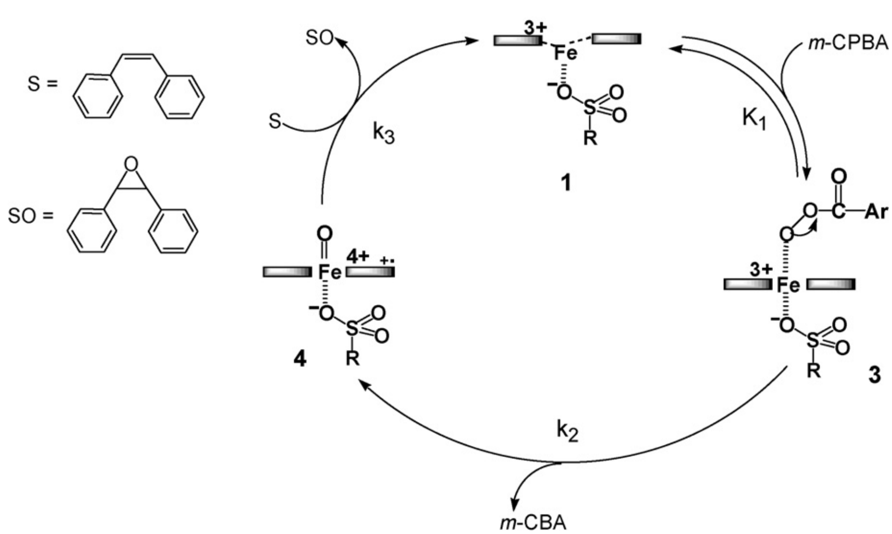

Scheme 14.

Acknowledgments

The author gratefully acknowledges financial support from the Deutsche Forschungsgemeinschaft (SFB 583 and SPP 1118), Fonds der Chemischen Industrie, Max-Buchner-Forschungsstiftung, Alexander von Humboldt Foundation and DAAD.

References

[1] (a) R. van Eldik, C. Dücker-Benfer, F. Thaler, Adv. Inorg. Chem. 49 (2000) 1;
(b) C.D. Hubbard, R. van Eldik, in: M. Riad Manaa (Ed.), Chemistry at Extreme Conditions, Elsevier, Amsterdam, 2005, p. 109, Chapter 4;
(c) C.D. Hubbard, R. van Eldik, J. Coord. Chem. 60 (2007) 1–51, invited review.
[2] Anon., Special issue on inorganic and bioinorganic mechanisms, Chem. Rev. 105 (2005) 1917.
[3] L. Helm, A.E. Merbach, Chem. Rev. 105 (2005) 1923.
[4] T.W. Swaddle, A.E. Merbach, Inorg. Chem. 20 (1981) 4212.
[5] R. Puchta, N. van Eikema Hommes, R. van Eldik, submitted for publication.
[6] A. Cusanelli, U. Frey, D.T. Richens, A.E. Merbach, J. Am. Chem. Soc. 118 (1996) 5265.
[7] R. van Eldik, in: P. Warneck (Ed.), Heterogeneous and Liquid-Phase Processes, Springer, Berlin, 1995, p. 11, Chapter 2.
[8] C. Brandt, R. van Eldik, Chem. Rev. 95 (1995) 119–190.
[9] C. Brandt, I. Fabian, R. van Eldik, Inorg. Chem. 33 (1994) 687.
[10] (a) N. Coichev, R. van Eldik, J. Chem. Educ. 71 (1994) 767;
(b) H.D. Moya, E.A. Neves, N. Coichev, J. Chem. Educ. 76 (1999) 930.
[11] T. Schneppensieper, A. Zahl, R. van Eldik, Angew. Chem. Int. Ed. 40 (2001) 1678.
[12] M. Wolak, R. van Eldik, J. Am. Chem. Soc. 127 (2005) 13312.
[13] J.-E. Jee, S. Eigler, F. Hampel, N. Jux, M. Wolak, A. Zahl, G. Stochel, R. van Eldik, Inorg. Chem. 44 (2005) 7717.
[14] J.-E. Jee, M. Wolak, D. Balbinot, N. Jux, A. Zahl, R. van Eldik, Inorg. Chem. 45 (2006) 1326.
[15] A. Franke, G. Stochel, C. Jung, R. van Eldik, J. Am. Chem. Soc. 126 (2004) 4181.
[16] E.C. Constable, G. Braun, E. Bill, R. Dyson, R. van Eldik, D. Fenske, S. Kaderli, D. Morris, A. Neubrand, M. Neuburger, D.R. Smith, K. Wieghardt, M. Zehnder, A.D. Zuberbühler, Chem. Eur. J. 5 (1999) 498, and references cited therein.
[17] N. Suzuki, T. Higuchi, Y. Urano, K. Kikuchi, T. Uchida, M. Mukai, T. Kitagawa, T. Nagano, J. Am. Chem. Soc. 122 (2000) 12059.
[18] W.-D. Woggon, Acc. Chem. Res. 38 (2005) 127.
[19] A. Franke, G. Stochel, N. Suzuki, T. Higuchi, K. Okuzono, R. van Eldik, J. Am. Chem. Soc. 127 (2005) 5360.
[20] A. Franke, N. Hessenauer-Ilicheva, D. Meyer, G. Stochel, W.-D. Woggon, R. van Eldik, J. Am. Chem. Soc. 128 (2006) 13611.
[21] M. Wolak, R. van Eldik, Chem. Eur. J., literature cited therein, in press.
[22] L.G. Denisov, T.M. Makris, S.G. Sligar, I. Schlichting, Chem. Rev. 105 (2005) 2253.
[23] M. Wolak, A. Theodoridis, A. Brausam, R. van Eldik, work in progress.
[24] N. Hessenauer-Ilicheva, A. Franke, D. Meyer, W.-D. Woggon, R. van Eldik, submitted for publication.